Aachen Institute for Advanced Study in Computational Engineering Science

Preprint: AICES-2008-16

6/April/2008

Model discrimination for the propionic acid diffusion into hydrogel beads using lifetime confocal laser scanning microscopy

A. C. Spiess, M. Zavrel, M. B. Ansorge-Schumacher, C. Janzend,

C. Michalik, T. W. Schmidt, etc.

RWTH AACHEN UNIVERSITY

AICES

Financial support from the Deutsche Forschungsgemeinschaft (German Research Association) through grant GSC 111 is gratefully acknowledged.

©A. C. Spiess, M. Zavrel, M. B. Ansorge-Schumacher, C. Janzend, C. Michalik, T. W. Schmidt, etc. 2008. All rights reserved
List of AICES technical reports: http://www.aices.rwth-aachen.de/preprints

Author's personal copy

Chemical Engineering Science 63 (2008) 3457 – 3465

Contents lists available at ScienceDirect

Chemical Engineering Science

journal homepage: www.elsevier.com/locate/ces

Model discrimination for the propionic acid diffusion into hydrogel beads using lifetime confocal laser scanning microscopy

Antje C. Spiess[a,*], Michael Zavrel[a], Marion B. Ansorge-Schumacher[b,c], Christoph Janzen[d], Claas Michalik[e], Thomas W. Schmidt[b], Tilman Schwendt[d], Jochen Büchs[a], Reinhart Poprawe[d], Wolfgang Marquardt[e]

[a]*Lehrstuhl für Bioverfahrenstechnik, RWTH Aachen, Worringerweg 1, D-52056 Aachen, Germany*
[b]*Lehrstuhl für Biotechnologie, RWTH Aachen, Worringerweg 1, D-52056 Aachen, Germany*
[c]*Enzymtechnologie, Institut für Chemie, TU Berlin, Straße des 17. Juni 124-128, D-10623 Berlin, Germany*
[d]*Lehrstuhl für Lasertechnik, RWTH Aachen, Fraunhofer Institut für Lasertechnik, Steinbachstr. 15, D-52074 Aachen, Germany*
[e]*Lehrstuhl für Prozesstechnik, RWTH Aachen, Turmstr. 46, D-52056 Aachen, Germany*

ARTICLE INFO

Article history:
Received 19 November 2007
Received in revised form 26 March 2008
Accepted 3 April 2008
Available online 6 April 2008

Keywords:
Biochemical engineering
Diffusion
Gels
Mathematical modelling
Model discrimination
Confocal laser scanning microscopy

ABSTRACT

Hydrogels are increasingly used for the entrapment of biocatalysts, especially for the use of enzymes in organic solvent systems. Hence, it is necessary to understand the influence of the hydrogel matrix on the transport kinetics (diffusion and phase transfer) and on the reaction kinetics (activity and stability of the enzymes). Here, the diffusion of propionic acid into Ca-alginate hydrogel beads is studied using a structured methodology, *m*odel-based *ex*perimental *a*nalysis (MEXA).

The basis for all further investigations is a rigorous model of all processes occurring during the diffusion of the propionic acid into the Ca-alginate hydrogel bead. As competing model assumptions the Fickian and Nernst–Planck diffusion laws are integrated. Then, an optimal experimental design is performed to determine those experiments that allow an efficient discrimination of the rival model candidates. The change in pH-value over time resulting from the diffusion of propionic acid into the hydrogel bead is observed in the centre of the hydrogel bead. The fluorescent pH-indicator resorufin shows pH-dependent lifetimes that are measured by time-correlated single photon counting using a confocal laser scanning microscope at high temporal resolution (every 1 s). To our knowledge lifetime confocal laser scanning microscopy is used for the first time in this study for the quantification of dynamic pH-changes in macroscopically large particles. The model parameters for each candidate model are estimated based on 16 independent experimental data sets. Finally, the likelihood function is used to evaluate and discriminate the competing diffusion laws.

For the diffusion of propionic acid into spherical Ca-alginate hydrogel beads, it could be shown that Fickian diffusion is not able to describe the process accurately in contrast to Nernst–Planck diffusion. The influence of the Ca-alginate hydrogel density was found to be insignificant for the estimated diffusion coefficient.

© 2008 Elsevier Ltd. All rights reserved.

1. Introduction

Nowadays, biocatalysis can be considered as an established tool to produce bulk and fine chemicals, where a strong focus lies on chiral precursors and active pharmaceuticals (Liese et al., 2000; Schmid et al., 2001; Schoemaker et al., 2003). For some substrates and products the solubility in the natural aqueous environment of the enzymes is limiting (Leresche and Meyer, 2006). To this end, the natural, aqueous medium is exchanged against a so called non-conventional medium, often an organic solvent (Hudson et al., 2005). The stabilisation of enzymes for those environments is frequently accomplished by immobilisation, eventually limiting the rate of the enzyme catalysed reaction by substrate diffusion. The entrapment of enzymes into macroscopic hydrogel beads provides a stabilised aqueous environment for the enzyme while being suspended in an organic solvent. This forms a generic solution that can easily be adapted to a wide range of enzymes (Ansorge-Schumacher et al., 2000; Metrangolo-Ruiz et al., 2005). However, the microenvironment of the enzyme is inevitably influenced by any type of hydrogel.

A rational design of hydrogel matrices requires the mechanistic understanding of all effects occurring in an immobilised biocatalyst

* Corresponding author. Tel.: +49 241 80 28111; fax: +49 241 80 22265.
E-mail address: antje.spiess@avt.rwth-aachen.de (A.C. Spiess).

0009-2509/$ - see front matter © 2008 Elsevier Ltd. All rights reserved.
doi:10.1016/j.ces.2008.04.005

Author's personal copy

reaction system. One basic description for reaction–diffusion coupling is the Thiele modulus that relates the maximum reaction velocity of the enzyme to the diffusivity of the substrate, indicating regimes of reaction or diffusion control. When immobilising enzymes, the activity loss due to diffusion limitation is often expressed as effectiveness factor, the ratio of observed activity of the immobilised enzyme over that of the free enzyme. For the simplified case of Fickian diffusion and irreversible Michaelis–Menten kinetics, analytical solutions for the effectiveness factor are available (Buchholz et al., 2005). However, this simplified approach to diffusion necessarily fails if the above assumptions do not hold, or if additional interactions inside the hydrogel matrix occur. Examples for those additional complications include an uneven enzyme distribution across the catalyst radius (Hossain and Do, 1992), or pH- and substrate concentration gradients influencing the reaction kinetics and/or the selectivity (Bailey and Chow, 1974; Spiess and Kasche, 2001; Berendsen et al., 2006). To account for more complex kinetics with electrolytes as reactants, a distributed model incorporating Nernst–Planck diffusion for infinitely dilute aqueous electrolytes and a radial enzyme gradient has recently been explored (van Roon et al., 2006).

Traditionally concentration measurements over time in the bulk phase are used to evaluate both the reaction rates and the diffusion coefficients inside the hydrogel matrix (Polakovic et al., 2001). This integral information is not considered sufficient to quantify the local effects of the hydrogel matrix on both reaction and transport kinetics. Thus, additional measurements inside the carrier are required. Spectroscopic measurement techniques are increasingly applied for the non-invasive in situ observation of chemical species. Due to recent developments of different concentration quantification methods a detailed observation of transport processes is now possible. Nuclear magnetic resonance (NMR) techniques have recently been applied for the imaging of transport phenomena and chemical reactions (Küppers et al., 2002). In principle, any chemical species can be observed using NMR imaging. However, a severe trade-off between spatial, chemical and temporal resolution exists. Therefore the resolution of species concentrations during fast transients is currently limited. Raman spectroscopy has also been used for the spatially resolved observation of concentration and for the determination of diffusion coefficients in hydrogel slabs (Kwak and Lafleur, 2003). The applicability of Raman spectroscopy; however, is limited because only non-fluorescent species of significant concentration can be quantified so far. In contrast, the widely applied confocal laser scanning microscopy (CLSM) can only observe fluorescent species. Therefore, CLSM requires either fluorescent molecules (Tallarek et al., 2003; Cvetkovic and Straathof, 2004), or small fluorescent marker molecules attached to macromolecules to allow for spatially resolved concentration measurements (Kasche et al., 2003). The quantification of concentration based on fluorescence intensity; however, has been demonstrated to be limited by the attenuation of light by the carrier matrix that results in depth-dependent calibration curves and prohibits the evaluation of (fast) dynamic diffusion problems (Heinemann et al., 2004). The impact of light attenuation may be overcome using either two-photon excitation (Denk et al., 1990), or fluorescence lifetime CLSM (Kuwana et al., 2004). Comparing the available spectroscopic techniques, the highest potential for diffusion measurements in transparent hydrogel matrices is attributed to CLSM due to its high temporal and spatial resolution and the availability of suitable indicators.

The objective of the present work is to discriminate between possible diffusion laws for the diffusion of propionic acid into Ca-alginate hydrogels. Propionic acid is an example for dissociating species, which can be quantified using a fluorescent pH-indicator detected by lifetime CLSM. Due to the complexity of the experimentation equipment and the specificity of the questions raised, model-based experimental analysis (MEXA) is used to guide the work process.

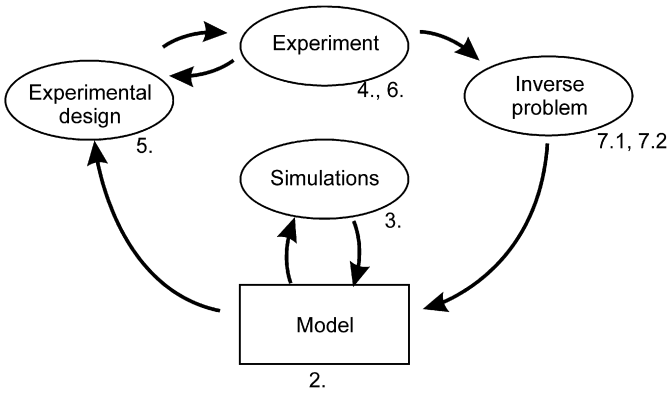

Fig. 1. Model-based experimental analysis work flow as applied in this paper. The numbers in the figure indicate the respective section numbers.

The methodology has been developed to provide a systematic framework that optimally combines modelling, experimentation and the solution of inverse problems for the evaluation of experimental data (Marquardt, 2005). A simplified scheme of the sequential modelling, experimental, and evaluation steps, taken during this work, is given in Fig. 1 and guides through this paper.

After the initial development of the diffusion model variants (Section 2), the MEXA cycle is passed twice. Simulations are performed to check for identifiability and discriminability of some of the model variants (Section 3). Constrained by the available experimental methods and equipments (Section 4), the optimal experiments for model discrimination are determined (Section 5). The experimental results (Section 6) are then used for the estimation of the diffusion parameters for both model variants and for the model discrimination, i.e. for the performance comparison of both models (Section 7.1). Due to an unexpected result, the model candidates are analysed and re-formulated and the parameter estimation procedure is repeated (Section 7.2).

2. Model development

The system of interest is an enzyme catalysed esterification reaction in Ca-alginate beads suspended in an organic solvent that serves as substrate supply. The hydrogel matrix consists of Ca-alginate, which results from the gelation of alginate with $CaCl_2$, releasing free chloride (Cl^-) ions during cross-linking. The Ca-alginate matrix is considered immobile, but is slightly buffered using Tris buffer to control the pH-value during gelation. The Cl^- anion, the excess calcium ions, as well as Tris and $TrisH^+$ are supposed to be mobile. In an esterification reaction, the acid reactant may dissociate to the corresponding basic anion. The diffusion of a charged compound can show differences between the Fickian and Nernst–Planck diffusion laws. Thus, the diffusion of propionic acid (HPa) and its propionate anion (Pa^-) in the hydrogel matrix is investigated.

Assuming an ideally mixed batch system without volume change and ideally spherical particles, the mass balance equations for the bulk and the bead read as follows:

$$V^{\text{bulk}} \frac{\mathrm{d}c_i^{\text{bulk}}}{\mathrm{d}t} = k_{L,i} \cdot A^{\text{bead}} \cdot (P_i \cdot c_i^{\text{bead}} - c_i^{\text{bulk}}) \tag{1}$$

$$\frac{\partial c_i^{\text{bead}}}{\partial t} = -\frac{1}{r^2}\left(\frac{\partial}{\partial r} \cdot r^2 \cdot j_i\right) \tag{2}$$

Author's personal copy

with the following boundary and initial conditions:

$$r = 0 : \frac{\partial c_i}{\partial r} = 0$$

$$r = R : -j_i = k_{L,i} \cdot \left(\frac{c_i^{\text{bulk}}}{P_i} - c_i^{\text{bead}} \right), \quad i = \text{HPa} \tag{3}$$

$$t = 0 : c_i^{\text{bulk}} = c_{i,0}^{\text{bulk}}, \quad c_i^{\text{bead}} = c_{i,0}^{\text{bead}} \tag{4}$$

where V^{bulk} represents the volume of the bulk phase, c_i the concentrations in the bead and the bulk phase, respectively, $k_{L,i}$ the mass transfer coefficients, A^{bead} the surface of the bead and P_i the partition coefficient between the phases.

The diffusion velocity of charged species at constant pressure may be described using Nernst–Planck law (Taylor and Krishna, 1993), where the area-specific flux of a charged component is driven by a combination of the gradients in concentration and electrical potential:

$$j_i = -D_i \cdot \left(\frac{\partial c_i}{\partial r} + z_i \cdot c_i \frac{F}{R_m T} \frac{\partial \Phi}{\partial r} \right) \tag{5}$$

where i denotes the diffusing species, j_i is the molar diffusive flux (in $\text{mol m}^{-2}\,\text{s}^{-1}$), D_i the effective diffusion coefficient in the alginate matrix, c_i the local concentration, r the radial position in the bead, z_i the charge, F the Faraday constant, R_m the gas constant, T the temperature, and Φ the electrical potential. The gradient in potential can be expressed in terms of concentrations by summing up the concentration gradients of all involved species. This yields a representation of Nernst–Planck law based merely on ion concentrations, ion diffusivities and ion charges (Taylor and Krishna, 1993):

$$j_i = -D_i \cdot \frac{\partial c_i}{\partial r} - \frac{z_i \cdot D_i \cdot c_i}{\sum_h z_h^2 \cdot D_h \cdot c_h} \cdot \sum_h z_h \cdot D_h \cdot \frac{\partial c_h}{\partial r} \tag{6}$$

For uncharged species ($z_i = 0$), the second summand equals zero, resulting in Fick's law:

$$j_i = -D_i \cdot \frac{\partial c_i}{\partial r} \tag{7}$$

As stated above, the diffusing species are electrolytes that may dissociate depending on the environment. The dissociation process is fast in comparison to the diffusion. Therefore, it is assumed that the dissociation reaction is in equilibrium at all times. The dissociation equilibrium is represented by the mass action laws:

$$K_i = \frac{c_{i,\text{cation}} \cdot c_{i,\text{anion}}}{c_{i,\text{electrolyte}}} \tag{8a}$$

$$K_W = c_{\text{H}+} \cdot c_{\text{OH}-} \tag{8b}$$

where K_i is the dissociation constant, the c_i's are the concentrations of the undissociated electrolytes, the cation, and the anion, respectively, while K_W is the ion product of water, $c_{\text{H}+}$ the proton, and $c_{\text{OH}-}$ the hydroxide ion concentration. Since electroneutrality is given at all times, expressed by the charge balance,

$$\sum_i c_i \cdot z_i = 0 \tag{9}$$

one diffusive flux can be expressed through the diffusion of all other species.

The diffusion coefficient D_i in the hydrogel bead matrix is dependent on the alginate density. However, the Ca-alginate beads are not homogeneous, but the alginate polymer is radially distributed. During the gelling process, the multivalent Ca-ions diffuse from the surface and rapidly cross-link, resulting in a higher concentration near the surface than in the core (Thu et al., 2000). For the bead production process used in this work, the alginate density distribution has been measured using Raman spectroscopy (Heinemann et al., 2005). A quadratic equation was used to fit the alginate density profile:

$$w_{\text{Alg}}(r) = \overline{w}_{\text{Alg}} + d \cdot (r^2 - \tfrac{3}{5} \cdot R^2) \tag{10}$$

where w_{Alg} is the alginate concentration, $\overline{w}_{\text{Alg}}$ the average alginate concentration, d a model parameter to be fitted, and R the bead radius. Masaro and Zhu (1999) list several physical models mainly for self-diffusion of small to medium sized non-electrolytes in polymer solutions in their review article. The presented model alternatives express the diffusion coefficient (D_i) as a function of the diffusion coefficient in free solution ($D_{i,0}$) and a tuneable model parameter (k). The most simplified models take exponential (hydrodynamic theory, model of Gao and Fagerness, Eq. (11a)), hyperbolic (simplified Maxwell–Fricke model, Eq. (11b)), or linear form (obstruction model for micro-emulsions, Eq. (11c)), and are expressed in terms of the alginate concentration:

$$D_i = D_{i,0} \cdot \text{e}^{-k \cdot w_{\text{Alg}}} \tag{11a}$$

$$D_i = \frac{D_{i,0}}{1 + k \cdot w_{\text{Alg}}} \tag{11b}$$

$$D_i = D_{i,0} \cdot (1 - k \cdot w_{\text{Alg}}) \tag{11c}$$

where $D_{i,0}$ is here the diffusion coefficient in free solution and k a fitting parameter for the polymer diffusion model that indicates the extent of the matrix interaction.

3. Discriminability between diffusion parameter models (Eqs. (11a)–(11c))

Before any kind of model analysis (as for instance checking the model discriminability) can be performed, nominal values have to be assigned to all model parameters. An overview of the model parameters and the assigned values is provided in Table 1. Assuming a pH-range between 3 and 8 during the diffusion process, the very strong acid HCl is fully dissociated. Also most salt species are fully dissociated. To reduce the computational load, species that only occur theoretically are omitted in the model.

Table 1
Model parameters describing the diffusion of propionic acid into Ca-alginate hydrogel beads (Heinemann, 2003). (A) diffusion coefficients, (B) dissociation constants and (C) ion product of water

(A)	
Species	Diffusion coefficient, $D_{i,0}$ (m/s^2)
HPa	1.061 e−9
Pa^-	0.953 e−9
TrisH^+	0.778 e−9
Tris	0.7 e−9
CaCl^+	1 e−9
Ca^{2+}	0.792 e−9
Cl^-	2.032 e−9
OH^-	5.273 e−9
H^+	9.312 e−9
(B)	
Dissociation pair	Dissociation constants, $\text{p}K_i = \log K_i$
HPa/Pa^-	4.86
TrisH^+/Tris	8
(C)	
Dissociation pair	Ion product of water, $\text{p}K_w = \log K_w$
$\text{H}_2\text{O/OH}^-$	13.996

Author's personal copy

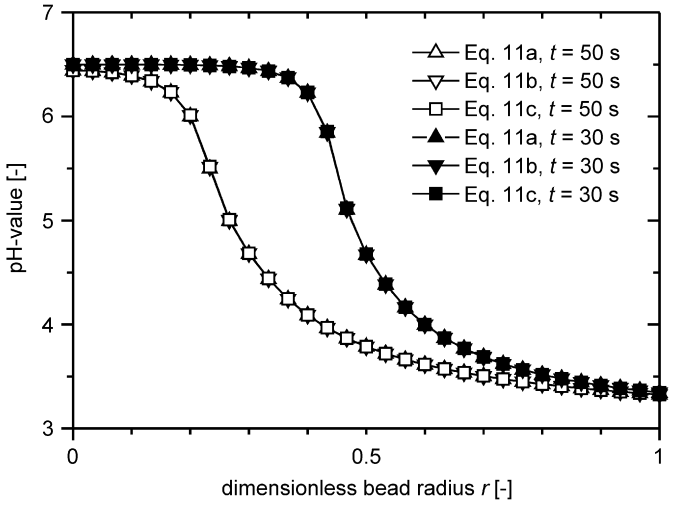

Fig. 2. Simulated pH-value over time in the hydrogel particle core after 30 and 50 s assuming different (linear, exponential, hyperbolic) dependence of the diffusion coefficient on the local alginate density (Eqs. (11a)–(11c)). Nernst–Planck diffusion is chosen as diffusion model. Simulation parameters: $R = 1.15$ mm, $pH_{bead,0} = 6.5$, $c_{Pa,tot,0} = 100$ mM.

The discriminability of the diffusion law variants (different assumptions on the dependence of the effective diffusion coefficient on the alginate density, Eqs. (11a)–(11c), hereafter referred to as alternative diffusion models) is investigated simulating the pH-profiles under identical initial conditions. For the subsequent simulations, the following realistic parameter values have been used: The nominal bead radius R is set to 1.15 mm. The hydrogel beads contain $\overline{w}_{Alg} = 3.3\%$ (w/w) sodium alginate in 50 mM Tris buffer and have been hardened with $CaCl_2$ to yield a bead concentration of 180 mM $CaCl_2$. The alginate distribution has been fitted to measured alginate concentration profiles (Heinemann et al., 2005), giving an alginate parameter $d = 6000\,g\,g^{-1}\,m^{-2}$ (see Eq. (10)). The initial pH-value of the beads is set to $pH_0 = 6.5$ and the volume of the bulk solution to $V^{bulk} = 300\,\mu L$. The initial total concentration of propionic acid $c_{Pa,tot,0}$ is set to 100 mM . The calculated influence of the alternative diffusion coefficient models (Eqs. (11a)–(11c)) on the effective diffusion coefficient and thus the resulting pH-profiles at different times using Nernst–Planck law is shown in Fig. 2.

These simulations show no visible difference in the pH-profiles calculated for the alternative diffusion coefficient models Eq. (11). Inspecting the numerical data, the largest simulated difference occurs at the centre of the bead where it amounts to less than 0.0066 pH-units. Even using highly accurate pH-measurement methods, these differences are an order of magnitude smaller than the typical measurement errors. Therefore, the simulations show that a discrimination of the alternative diffusion coefficient model variants for low molecular weight substrates cannot be expected using hydrogels of this density and size. In the following sections, the exponential dependence of the diffusion coefficient on alginate density (Eq. (11a)) was chosen to account for the radial variation of the diffusion coefficient and the task of model discrimination was re-focused to discrimination between Fick and Nernst–Planck diffusion only.

4. Experimental methods and calibration

4.1. Chemicals

Propionic acid, Tris base, and calcium chloride were purchased from Fluka, Buchs, CH. Resorufin was obtained from Sigma-Aldrich, Deisenhofen, Germany. Manugel DJX sodium alginate was purchased from Monsanto, San Diego, CA, US. All chemicals used were of analytical grade.

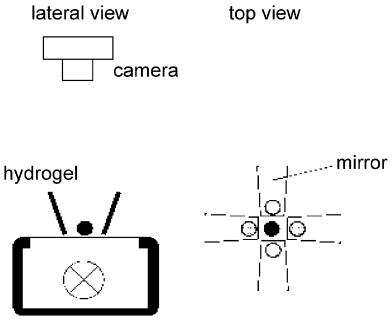

Fig. 3. Device for the determination of bead roundness. Digital pictures are taken from an illuminated hydrogel bead and its four mirror images and subsequently analysed quantitatively.

4.2. Preparation and characterisation of hydrogel beads

Two percent (w/v) sodium alginate was dissolved in 50 mM Tris buffer, pH 6.8. To obtain almost ideally round beads, each 15 μL of alginate solution were dropped into a column containing a Ca^{2+} and a density gradient (Buthe et al., 2004), resulting in beads of approximately 1 mm radius. The beads were washed several times with 50 mM Tris buffer containing 2% $CaCl_2$ and 500 μM resorufin as fluorescent lifetime pH-indicator. Bead diameter (as Feret-diameter) and roundness (as r_{min}/r_{max}) were measured using the device depicted in Fig. 3 and the image analysis software Image Tool 3.00 (UHTSCSA, San Antonio, TX, US).

4.3. Diffusion experiment

The diffusion experiments are performed in a 96-well microtiter plate at room temperature. To guarantee uniform conditions around the hydrogel bead, it is placed on top of a circular holder supporting the bead at three points above the well bottom. The diffusion experiment is initiated adding 300 μL of propionic acid $c_{Pa,tot,0} \sim 100$ mM to the well. Solvent evaporation was considered negligible due to the short duration of the experiment.

4.4. Control of beads

After each measurement, the position and the quality of the hydrogel bead is controlled using light microscopy. Data from beads that have not been centred correctly or that contained cracks or air inclusions are rejected. The beads are subsequently checked for diameter and roundness (see above). Beads with a roundness less than 0.8 are rejected likewise.

4.5. Measurement of pH-dependent resorufin lifetime using confocal laser scanning microscopy (CLSM)

For the lifetime measurements, a Leica TCS SP2 confocal laser scanning microscope (Leica Microsystems Heidelberg GmbH, Mannheim, Germany) has been combined with a pulsed 405 nm diode (PicoQuant, Berlin, Germany) emitting picosecond laser pulses for the excitation of resorufin fluorescence. Only fluorescence photons emitted from the confocal plane can pass a confocal pinhole and are collected through a longpass filter (edge 500 nm) by a photomultiplier tube (PMT) with high quantum efficiency and accurate timing characteristics (H7422P-40, Hamamatsu Photonics GmbH,

Author's personal copy

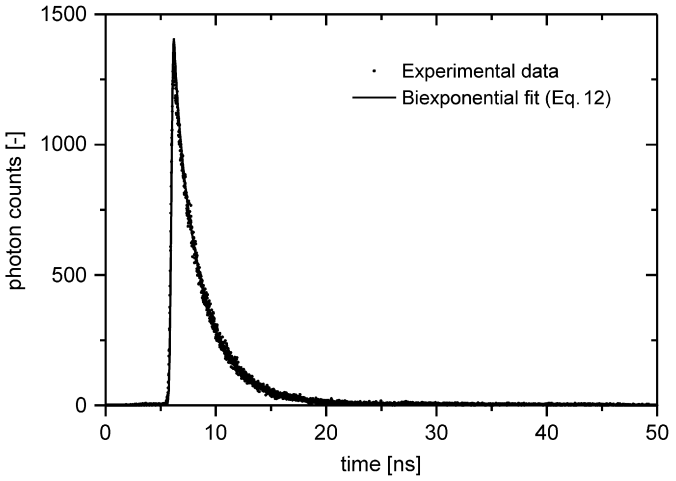

Fig. 4. Fluorescence intensity decay over time. Points correspond to photon counts during the calibration of resorufin in Ca-alginate hydrogel bead at pH 6.2. The line corresponds to the fitted biexponential decay curve. $\chi^2 < 1.3$ was obtained for all calibration fits.

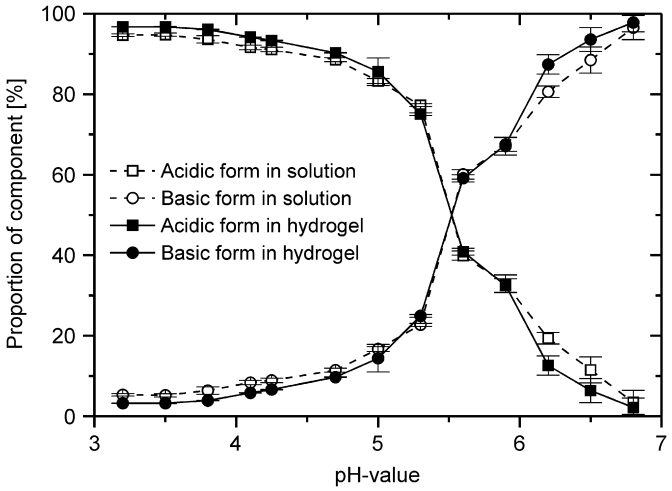

Fig. 5. Calibration of pH-value vs. the proportion of acidic and basic dissociation forms A (Square) and B (Circles) of resorufin as determined from biexponential decay curves. Open symbols indicate measurements in alginate solution, closed symbols refer to Ca-alginate hydrogel beads. The error bars indicate the standard deviation based on 10 repetitions of 30 s duration each.

Herrsching, Germany). The electrical pulses from the PMT are guided to an external PC-system with a fast electronics for photon counting (SPC 830, Becker and Hickl, Berlin, Germany), that correlates the counted photons to the excitation laser pulses via time-correlated single photon counting (TCSPC) and writes the results to a file. During all experiments, the average power of the laser diode was kept at 50 μW, and the repetition rate at 20 MHz. The diffusion experiment was observed for 300 s, divided into 300 observation cycles of 1 s each to balance time resolution with sufficient number of photons. During this second all recorded photons were accumulated to calculate one lifetime decay curve.

4.6. Calibration

For the calibration of the correlation between the pH-value and the resorufin fluorescence lifetime, resorufin-dotted sodium alginate solutions and Ca-alginate hydrogel beads were equilibrated at different pH-values. In each of those samples, the decay of resorufin intensity after the excitation pulses was recorded tenfold for 30 s duration using all wavelengths larger than 500 nm. The acidic and basic forms of resorufin have different pH-independent lifetimes (Ryder et al., 2003). At a defined pH-value, the decay curve is composed of lifetime components of both forms. Thus, a biexponential intensity decay over time will yield the proportion a and b of the acidic and basic component, respectively:

$$\mathrm{Int} = a \cdot \mathrm{e}^{-t/\tau_A} + b \cdot \mathrm{e}^{-t/\tau_B} \tag{12}$$

where Int is the normalised time-dependent intensity, t the time, a and b the pre-exponential factors that sum up to 1, and τ_A and τ_B the corresponding intrinsic lifetimes for the acidic and basic component, respectively. A typical intensity decay is shown in Fig. 4.

4.7. Calibration

Before carrying out the diffusion experiments, the dependence of the fluorescence lifetime of resorufin on the pH-value has to be determined. Please note that the calibration procedure also incorporates models that are treated separately from the diffusion process model. The lifetime curves of resorufin at the different pH-values are fitted using Eq. (12) with fixed lifetimes. The resulting proportion of acidic to basic component over pH-value in both the alginate solution and the hydrogel bead is depicted in Fig. 5.

Fig. 5 shows the typical shape of a pH-titration curve with a pK-value of approximately 5.6, where nearly pure acidic or basic form of the pH-indicator resorufin is observed at roughly 1.5 pH-units below and above the pK-value. This supports the assumption of biexponential decay using fixed lifetimes. The lifetimes of the acidic and basic component of 0.4 and 2.6 ns, respectively, coincide reasonably well with the data reported earlier of 0.3–0.67 and 3.3–3.4 ns (Ryder et al., 2003). The deviations may be due to the chosen excitation and observation wavelength ranges and the assumption of fixed component lifetimes across all pH-values. The standard deviation of the replicates is between 0.3% and 3%, with the higher error occurring at high pH-values. The increase of experimental error with increasing pH-value is due to the different intensity of both dissociating forms of resorufin. At basic pH-values, the anion with a lower intensity prevails, resulting in the lifetime decay curve consisting of fewer counted photons. The microenvironment of resorufin changes the lifetime only slightly. A somewhat steeper slope is observed for Ca-alginate beads in comparison to dissolved alginate. However, the error bars indicate that the difference is insignificant except for the pH-values 6.2 and 6.5. In independent experiments, it has been verified that the scanning depth in the hydrogel bead does not influence the lifetime measurement (data not shown).

The calibration curve for the acidic component A (Fig. 5) decreases monotonously with increasing pH-value; however, the curve shows a slight shoulder around pH 5.5. For the evaluation of the diffusion experiments, a linear interpolation between the calibration points is applied to estimate the pH-value.

5. Design of experiments for model discrimination

Based on the experimental set-up, the optimal experiments for discrimination between Fickian and Nernst–Planck diffusion can be designed. According to the simple approach of Hunter and Reiner (1965), an optimal experiment is defined as the one giving the largest difference between both competing model candidates. Numerically, this refers to the maximisation of the objective function $\Psi(\varphi)$ with respect to the experimental degrees of freedom φ:

$$\max_{\varphi} \Psi(\varphi) = \max_{\varphi} \int_{t=0}^{t=t_f} \sum_i [c_i^N(r,t,\theta^N,\varphi) - c_i^F(r,t,\theta^F,\varphi)]^2 \,\mathrm{d}t \tag{13}$$

Author's personal copy

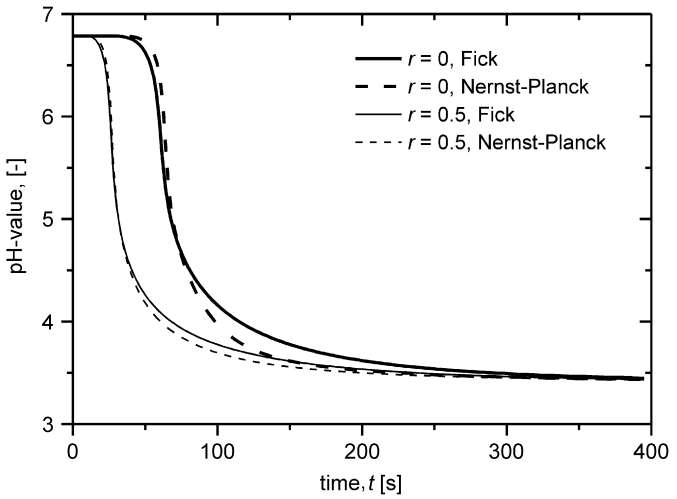

Fig. 6. Simulation of the development of pH-value over time at two different positions in a hydrogel bead: (thick) centre of the bead (r=0); (thin) middle between the centre and the surface of the bead ($r = 0.5$). Fickian (lines) and Nernst–Planck (dashes) diffusion are shown for an initial bulk phase concentration of 100 mM propionic acid into a Ca-alginate hydrogel bead of $R = 1.25$ mm radius with initial pH-value of 6.8.

where $\boldsymbol{\theta}^N$ and $\boldsymbol{\theta}^F$ are the parameter sets for Nernst-Planck and Fickia diffusion, respectively. The objective function integrates the predictions of concentration differences over time in order to determine the experimental conditions at which the model alternatives can be discriminated most efficiently. The experimental degrees of freedom for the optimisation are the measurement position r within the hydrogel bead, the hydrogel bead size, the initial pH-value of the bead, and the initial concentration of the propionic acid (and thus the initial pH-value in the bulk).

Regarding the optimal measurement position r during an experiment, different scanning strategies can be considered. The most simple approach is to measure for the whole time at a single, spatial position for the complete course of the reaction. Alternatively a scan along a line or across a plane is possible. The different scanning strategies might support the task of model discrimination differently well. Intuitively, measuring the concentration close to the diffusion front would be the optimal solution; however, this scanning strategy is not feasible with the device at hand and would require prior knowledge of the position of the diffusion front as a function of time. Simple line and plane scans may give additional information on the exact centring or the roundness of the bead, but this benefit comes at the cost of a lower time resolution. For these reasons we decided for the single point measurement strategy. Fig. 6 shows the pH profiles using the two alternative diffusion laws and different measurement positions.

The experimental set-up poses the following constraints to the optimisation problem:

- The diameter of the hydrogel bead has an upper limit of 1.25 mm due to the observable area of the CLSM (2×2 mm using an objective with ten fold magnification). On the other hand the preparation of the beads defines a minimal bead size of 1 mm in order to guarantee a sufficient roundness.
- The optimal initial pH-value of the hydrogel beads is limited by the choice of resorufin as fluorescent pH-indicator in the experimental set-up. The pH-sensitivity covers the range of 4.0–7.0 due to an apparent pK-value of resorufin of 5.6. To ensure staying within this range even in the case of small experimental deviations, the lower bound of the initial pH-value is set to 4.2 and the upper bound to 6.8.

Table 2
Degrees of freedom and results for the optimal experimental design

Degrees of freedom	Lower bound	Upper bound	Initial estimate	Optimised value
Measurement position	$0 * r$	r	$0.5 * r$	$0 * r$
Bead size (mm)	1	1.25	1	1
Initial pH-value	4.2	6.8	6.8	6.8
Initial total concentration of propionic acid (mM)	0	100	80	100

- The initial total concentration of propionic acid is limited by the sensitivity range of resorufin. If too high initial propionic acid concentration is applied, the pH-value drops too fast through the sensitive range, resulting in too few observations. Thus, an upper bound to $c_{\mathrm{Pa,tot,0}}$ was set at 100 mM while the lower bound is set to 0 mM .

The result of the optimisation using Eq. (13) for these experimental degrees of freedom, together with the lower and optimal bounds and the initial estimates, is given in Table 2.

The optimal measurement position is in the centre of the bead, which should have a radius of 1 mm. The initial pH-value within the bead should be as high as possible (6.8) just as the initial total concentration of propionic acid within the bulk, which has an optimal value of 100 mM .

6. Experimental results

6.1. Diffusion experiments

The diffusion of propionic acid into an alginate hydrogel bead is observed using the confocal laser scanning microscope. The correct particle position is verified by light microscopy after finishing the experiment. At the same time, beads showing irregularities, such as cracks and holes, are rejected. Sixteen sets of experimental data have been obtained using this procedure. One of them is presented in Fig. 7.

The pH-value at the bead centre remains approximately constant for a certain lag-phase, corresponding to the diffusion of propionic acid into the hydrogel bead. With appearance of the diffusion front in the bead centre, a steep drop of the pH-value occurs. Between pH 6.0 and 5.5, a shoulder can be observed. This corresponds to the pH-values where the calibration curve deviates from the sigmoidal shape (Fig. 5). Finally, the pH-value approximates 3.9, which corresponds to the initial pH-value in the bulk. The experimental errors of the pH-value are estimated by horizontal projection of the experimental error bars of the acidic and basic component to the calibration graph (Fig. 7).

7. Model discrimination and parameter estimation

7.1. First cycle, model discrimination

For discriminating the correct diffusion model using the experimental data, i.e. to identify the Fickian or Nernst-Planck diffusion as more suitable for describing the diffusion of propionic acid in Ca-alginate hydrogel beads, a suitable sequential strategy needs to be defined to determine the model parameters from the experimental data. First, the initial experimental values are verified for each individual experiment. This is necessary to account for the inevitable deviations of the experimental conditions from their nominal values. The initial pH-value of the beads is estimated from the first couple of data points. Then, the initial concentration of propionic acid is estimated from the last couple of data points, i.e. the equilibrium data after the diffusion process has stopped. Finally, the bead size is

Author's personal copy

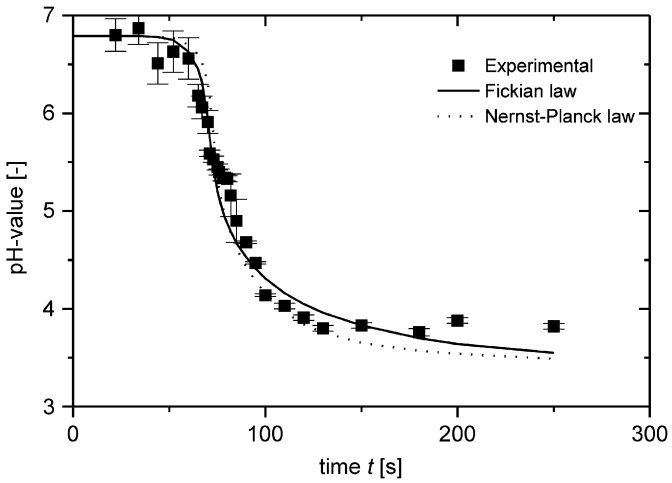

Fig. 7. Experimental (points) and estimated (lines) pH-values in the bead centre for the diffusion of propionic acid into Ca-alginate hydrogel beads. The initial model as described in Section 4 was used. Fickian diffusion is indicated as solid line, Nernst–Planck diffusion as dashed line. $R = 1.025$ mm. Estimated parameters: $pH_0 = 6.79$, $c_{Pa,tot,0} = 95$ mM, alginate influence parameter $k^F = 5.1$, $k^N = 6.6$.

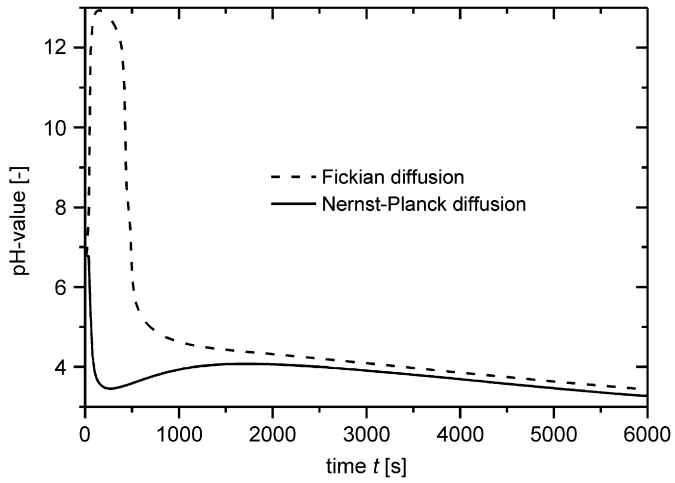

Fig. 8. Simulated pH progress in the bead centre for Fickian and Nernst–Planck diffusion. The corrected model as described in Section 7.2 was used.

estimated for each individual hydrogel bead within a range of ±2% around the optically determined Feret-diameter. These preliminary estimations of the experimental parameters help increasing the accuracy of the succeeding estimation of the model parameters. Outcome of this for the Fickian diffusion are initial pH-values inside the hydrogel bead between $pH_0 = 6.58$ and 6.76, initial total concentrations of propionic acid between 95 and 105 mM and bead radius between 1.02 and 1.13 mm.

Finally, all 16 experiments are simultaneously taken into account in order to estimate the parameter k in Eq. (11a) that accounts for the alginate density influence on the diffusion coefficient. The simulation results for the Fickian and the Nernst-Planck diffusion are demonstrated exemplarily in Fig. 7. The slope of the pH decrease over time was less steep for Fickian diffusion in comparison to Nernst-Planck diffusion and apparently better fitted the experimental data. The steeper slope for Nernst-Planck diffusion was reproducible for all hydrogel beads. It is attributed to the charge-mediated co-transport of ions resulting in a sharper diffusion front. The evaluation of the objective function for the parameter estimation shows that the value is slightly higher for Nernst-Planck diffusion than for Fickian diffusion, suggesting the latter as the better diffusion law.

Although only effective diffusion coefficients were estimated and multi-component effects were neglected due to the dilute nature of the system, it was surprising that Fickian diffusion was superior to Nernst Planck in modelling the diffusion of propionic acid into Ca-alginate hydrogel beads. Nernst-Planck diffusion was expected to be more suitable for modelling electrolyte diffusion in aqueous environments. One potential explanation was that the Ca-alginate hydrogel that consists of polyalginic acids cross-linked by bivalent Ca-ions, might be responsible for a high intrinsic ionic strength that overrules the charge co-transport. An estimation of the ionic strength; however, based on the alginate concentration of 3.3% (w/w) alginate gave a local monovalent alginic acid concentration of only 18 mM. $CaCl_2$ was present in concentrations of 180 mM, resulting in an ionic strength due to the alginate hydrogel of $I_{Alg} \sim 1$ M, a high value, but not sufficient to exclude charge interactions.

The resulting parameters describing the exponential density influence of the alginate matrix onto the effective diffusion coefficient were in the same order of magnitude for both diffusion models and amounted to $k^F = 5.1\,g\,g^{-1}$ for Fickian diffusion, in contrast to $k^N = 6.6\,g\,g^{-1}$ for Nernst–Planck diffusion, indicating slightly less influence of alginate hydrogel matrix in case of Fickian diffusion. Considering Eq. (11a) the overall diffusion coefficient in the hydrogel is in the order of 85% of the one in free solution indicating a strong reduction in comparison with the free diffusion due to the hydrogel matrix.

As a consequence of the remaining doubts, a detailed analysis of the model assumptions was undertaken. Although the investigation of the transport kinetics inside the hydrogel bead had the application of the hydrogel suspended in organic solvents in mind, the experiment was carried out in aqueous environment. This eliminated the need of refractivity index matching and also reduced the model complexity, because no phase equilibria on the phase boundary (Heinemann et al., 2003) had to be taken into account. With elimination of the organic solvent, however, one restriction regarding the mass transfer, i.e. that only uncharged components can cross the phase boundary, was overcome (refer to Eq. (3)). This restriction leads to the similarity of the simulated diffusion process for both Fickian and Nernst–Planck model. If organic solvents would have been used as a bulk phase for the diffusion measurements, the two competing diffusion models could not have been efficiently discriminated.

7.2. Second cycle, model improvement and final parameter estimation

The model was adjusted by allowing the mass transfer across the boundary layer(s) for all species, not only for the uncharged species. The mass transfer coefficients $k_{L,i}$ were related to the respective diffusion coefficients by the Sherwood number Sh which is assumed to be 2 in the unstirred case. The simulation with the unrestricted model results in a pH progress curve comparable to the previously simulated curves for Nernst–Planck diffusion. However, the simulation gives a significantly different result for Fickian diffusion, as shown in Fig. 8.

Obviously, Fickian diffusion is no longer capable of describing the experimentally observed diffusion process in accordance with the physical understanding of the system. In the modified model, the diffusion of all species across the phase boundary is possible, resulting in the diffusion of 360 mM chloride from the bead to the bulk with significantly higher diffusion coefficient (see D_i in Table 1) than the diffusion of 100 mM propionic acid from the bulk to the bead. Fick's law does not consider the co-transport of charged compounds that enhances or slows down the diffusional transport of other charged species. Instead, electroneutrality in the model is only achieved by

Author's personal copy

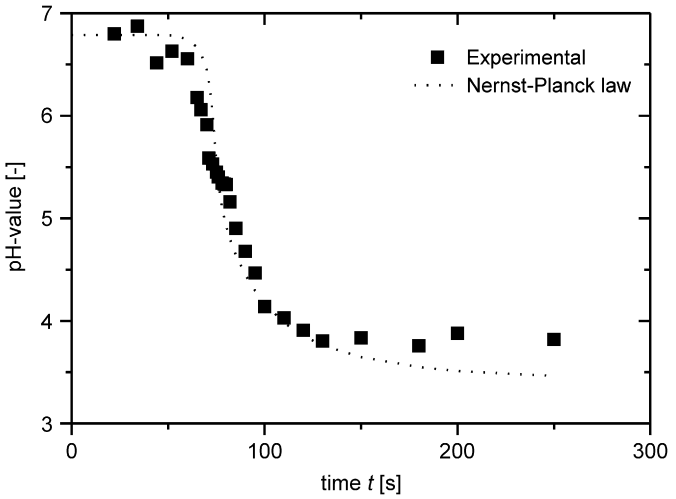

Fig. 9. Experimental (points) and estimated (dash) pH-values in the bead centre over time for the diffusion of propionic acid into Ca-alginate hydrogel beads. The corrected model as described in Section 7.2 was used. $R = 1.005$ mm, Estimated parameters: $pH_0 = 6.79$, $c_{Pa,tot,0} = 99.1$ mM, alginate influence parameter on diffusion $k = 0.051$.

water dissociation, resulting in an apparent disappearance of the strong hydrochloric acid from the bead. Only after 400 s, the pH-value inside the bead decreases again, to proceed to the same equilibrium value after long times. This behaviour is in contrast to the measurement data, supporting the use of the adequate diffusion model for electrolyte species. In the case of Nernst–Planck diffusion, the chloride diffusion does not occur independently of adequate counter-ion diffusion, resulting in a reasonable simulation profile (Fig. 9).

Using the new model, the measurement data are, again, explained well by the model. The key difference is found in the estimated parameters. The estimated parameter k that describes the influence of the alginate density on the diffusion coefficient is now estimated two orders of magnitude lower, $k \approx 0.02$, and is statistically no longer significant. Obviously, the alginate matrix does not pose a diffusion barrier to small molecules that serve as typical substrates for industrial fine chemical synthesis. This result is finally in accordance with earlier observations, where an alginate influence was observed only for molecules $> 20,000$ Da (Tanaka et al., 1984).

8. Conclusion

The objective of this paper was the discrimination of diffusion laws to describe the diffusion of propionic acid from bulk into Ca-alginate hydrogel beads. The simple model system was chosen for demonstrating steps towards a rational design of biocatalysis using hydrogels in organic solvent. To our knowledge lifetime CLSM was used for the first time in this study for the quantification of dynamic pH-changes in macroscopically large particles. The lifetime signal was not influenced by photon loss due to scattering and was found to be constant throughout the bead diameter. Calibration resulted in sigmoidal shaped component profiles vs. pH. As experimental setup, the diffusion from the bulk solution into a hydrogel bead fixed on a circular holder in a MTP well was chosen that allows a fast screening of hydrogel variants. A mathematical model was developed describing the effective diffusion of propionic acid from unstirred bulk solution into the hydrogel bead without taking multi-component effects into account. In case of diffusion from an aqueous bulk, the Fickian diffusion model could not adequately describe the experimentally obtained data, in contrast to the Nernst–Planck diffusion model. For small molecules, the Ca-alginate hydrogel matrix had no influence on the effective diffusion coefficient, but the diffusion coefficient was equal to a liquid system.

Along the investigation of the diffusion of propionic acid, this paper also illustrates the use of MEXA. Therefore, one detour made during the modelling process was shown that demonstrates that Fickian and Nernst–Planck diffusion models cannot be discriminated in the original hydrogel/organic solvent system, but only using an aqueous bulk solution. Thus, the potential of a structured work process to systematically identify suitable models was demonstrated. The approach will be further pursued for the simultaneous identification of diffusion and reaction using observed concentration profiles inside the catalyst pellets.

Notation

A	surface area, m^2
a, b	proportion of acidic and basic component of resorufin, %
c	concentration, $mol\,m^{-3}$
d	alginate density parameter, $g\,g^{-1}\,m^{-2}$
D_i	effective diffusion coefficient, $m^2\,s^{-1}$
$D_{i,0}$	diffusion coefficient in free solution, $m^2\,s^{-1}$
F	Faraday constant, $C\,mol^{-1}$
I	ionic strength, M
Int	normalised intensity as a function of time, dimensionless
i, h	counting variable for species, dimensionless
j	diffusive flux, $mol\,m^{-2}\,s^{-1}$
k	parameter for alginate density influence on diffusion coefficient, dimensionless
$k_{L,i}$	mass transfer coefficient from liquid to hydrogel phase, $m\,s^{-1}$
K	equilibrium constant for dissociation, $mol\,m^{-3}$
K_w	ion product of water, $10^{19.996}\,mol^2\,m^{-6}$
pK	negative decadic logarithm of dissociation constant K, dimensionless
P_i	partition coefficient, dimensionless
r	radial length, m
R	hydrogel bead radius, m
R_m	molar gas constant, $8.314\,J\,mol^{-1}\,K^{-1}$
t	time, s
T	temperature, K
V	volume, m^3
w_{Alg}	weight fraction of alginate, $g\,g^{-1}$
z	charge, dimensionless

Greek letters

θ	parameter set, dimensionless
σ	standard deviation, dimensionless
τ	fluorescence lifetime of resorufin component, ns
Φ	electrical potential, V
φ	experimental degrees of freedom, dimensionless
Ψ	objective function for discrimination, dimensionless

Subscripts

0	initial conditions
f	final
H^+	proton
HPa	propionic acid
max	maximal
min	minimal
OH^-	hydroxide ion

Author's personal copy

Pa^-	propionate anion
Pa, tot	total amount of propionic acid and propionate

Superscripts

bead	hydrogel bead phase
bulk	bulk phase
F	Fickian diffusion
N	Nernst–Planck diffusion

Acknowledgement

The authors thank the German Research Foundation (DFG, Deutsche Forschungs-gemeinschaft) for financial support of the project within the framework of the Collaborative Research Centre 540 "Model-based experimental analysis of kinetic phenomena in fluid multiphase reactive systems".

References

Ansorge-Schumacher, M.B., Doumeche, B., Metrangolo, D., Hartmeier, W., 2000. Enzyme encapsulation for biocatalysis in organic solvents—new approaches to the stereoselective synthesis of pharmaceutical compounds. Minerva Biotecnologica 12, 265–269.

Bailey, J.E., Chow, M.T.C., 1974. Immobilized enzyme catalysis with reaction-generated pH change. Biotechnology and Bioengineering 16, 1345–1357.

Berendsen, W.R., Lapin, A., Reuss, M., 2006. Investigations of reaction kinetics for immobilized enzymes—identification of parameters in the presence of diffusion limitation. Biotechnology Progress 22, 1305–1312.

Buchholz, K., Kasche, V., Bornscheuer, U.T., 2005. Biocatalysts and Enzyme Technology. Wiley-VCH, Weinheim.

Buthe, A., Hartmeier, W., Ansorge-Schumacher, M.B., 2004. Preparation of alginate beads for analytical purpose by a novel solvent-based methods. In: Proceedings of the XII. International Workshop on Bioencapsulation, pp. 246–250.

Cvetkovic, A., Straathof, A.J.J., Hanlon, D.N., Van der Zwaag, S., Krishna, R., Van der Wielen, L.A.M., 2004. Quantifying anisotropic solute transport in protein crystals using 3-D laser scanning a confocal microscopy visualization. Biotechnology and Bioengineering 86, 389–398.

Denk, W., Strickler, J.H., Webb, W.W., 1990. 2-Photon laser scanning fluorescence microscopy. Science 248, 73–76.

Heinemann, M., 2003. Experimental analysis, modeling and dynamic simulation of thermodynamic and kinetic phenomena in gel-stabilized enzyme carriers. Dissertation, RWTH Aachen.

Heinemann, M., Kümmel, A., Giesen, R., Ansorge-Schumacher, M., Büchs, J., 2003. Experimental and theoretical analysis of phase equilibria in a two-phase system used for biocatalytic esterifications. Biocatalysis and Biotransformation 21, 115–121.

Heinemann, M., Limper, U., Büchs, J., 2004. New insights in the spatially resolved dynamic pH measurement in macroscopic large absorbent particles by confocal laser scanning microscopy. Journal of Chromatography A 1024, 45–53.

Heinemann, M., Meinberg, H., Büchs, J., Koss, H.-J., Ansorge-Schumacher, M.B., 2005. Method for quantitative determination of spatial polymer distribution in alginate beads using Raman spectroscopy. Applied Spectroscopy 59, 280–285.

Hossain, M.M., Do, D.D., 1992. Determination of intraparticle immobilized enzyme distribution under moderate diffusion conditions. Biotechnology and Bioengineering 40, 743–747.

Hudson, E.P., Eppler, R.K., Clark, D.S., 2005. Biocatalysis in semi-aqueous and nearly anhydrous conditions. Current Opinion is Biotechnology 16, 637–643.

Hunter, W.G., Reiner, A.M., 1965. Designs for discriminating between two rival models. Technometrics 7, 307.

Kasche, V., de Boer, M., Lazo, C., Gad, M., 2003. Direct observation of intraparticle equilibration and the rate-limiting step in adsorption of proteins in chromatographic adsorbents with confocal laser scanning microscopy. Journal of Chromatography B 790, 115–129.

Küppers, M., Heine, C., Han, S., Stapf, S., Blümich, B., 2002. In situ observation of diffusion and reaction dynamics in gel microreactors by chemically resolved NMR microscopy. Applied Magnetic Resonance 22, 235–246.

Kuwana, E., Liang, F., Sevick-Muraca, E.M., 2004. Fluorescence lifetime spectroscopy of a pH-sensitive dye encapsulated in hydrogel beads. Biotechnology Progress 20, 1561–1566.

Kwak, S., Lafleur, M., 2003. Raman spectroscopy as a tool for measuring mutual-diffusion coefficients in hydrogels. Applied Spectroscopy 57, 768–773.

Leresche, J.E., Meyer, H.-P., 2006. Chemocatalysis and biocatalysis biotransformation: some thoughts of a chemist and of a biotechnologist. Organic Process Research & Development 10, 572–580.

Liese, A., Seelbach, K., Wandrey, C., 2000. Industrial Biotransformations. Wiley-VCH, Weinheim.

Marquardt, W., 2005. Model-based experimental analysis of kinetic phenomena in multi-phase reactive systems. Transactions of the Institution of Chemical Engineers Part A, Research and Design 83 (A6), 561–573.

Masaro, L., Zhu, X.X., 1999. Physical models of diffusion for polymer solutions gels and solids. Progress in Polymer Science 24, 731–775.

Metrangolo-Ruiz De Temino, D., Hartmeier, W., Ansorge-Schumacher, M.B., 2005. Entrapment of the alcohol dehydrogenase from *Lactobacillus kefir* in polyvinyl alcohol for the synthesis of chiral hydrophobic alcohols in organic solvents. Enzyme and Microbiol Technology 36, 3–9.

Polakovic, M., Kudlacova, G., Stefuca, V., Bales, V., 2001. Determination of sucrose effective diffusivity and intrinsic rate constant of hydrolysis catalysed by Ca-alginate entrapped cells. Chemical Engineering Science 56, 459–466.

Ryder, A.G., Power, S., Glynn, T.J., 2003. Fluorescence lifetime based pH sensing using Resorufin. In: Glynn, T.J. (Ed.), Opto-Ireland 2002: Optics and Photonics Technologies and Applications. SPIE, pp. 827–835.

Schmid, A., Dordick, J.S., Hauer, B., Kiener, A., Wubbolts, M., Witholt, B., 2001. Industrial biocatalysis today and tomorrow. Nature 409, 258–268.

Schoemaker, H.E., Mink, D., Wubbolts, M.G., 2003. Dispelling the myths—biocatalysis in industrial synthesis. Science 299, 1695–1697.

Spiess, A.C., Kasche, V., 2001. Direct measurement of pH profiles in immobilized enzyme carriers during kinetically controlled synthesis using CLSM. Biotechnology Progress 17, 294–303.

Tallarek, U., Rapp, E., Sann, H., Reichl, U., Seidel-Morgenstern, A., 2003. Quantitative study of electrokinetic transport in porous media by confocal laser scanning microscopy. Langmuir 19, 4527–4531.

Tanaka, H., Matsumura, H., Veliky, I.A., 1984. Diffusion characteristics of substrates in Ca-alginate gel beads. Biotechnology and Bioengineering 26, 53–58.

Taylor, R., Krishna, R., 1993. Multicomponent mass transfer. Wiley, New York.

Thu, B., Gaserod, O., Paus, D., Mikkelsen, A., Skjak-Braek, G., Toffanin, R., Vittur, F., Rizzo, R., 2000. Inhomogeneous alginate gel spheres: an assessment of the polymer gradients by synchrotron radiation-induced X-ray emission, magnetic resonance microimaging, and mathematical modeling. Biopolymers 53, 60–71.

van Roon, J.L., Arntz, M.M.H.D., Kallenberg, A.I., Paasman, M.A., Tramper, J., Schroen, C.G.P.H., Beeftink, H.H., 2006. A multicomponent reaction–diffusion model of a heterogeneously distributed immobilized enzyme. Applied Microbiology and Biotechnology 72 (2), 263–278.